Int. J. Heat Mass Transfer. Vol. 36, No. 13, pp. 3271–3281, 1993
Printed in Great Britain

0017-9310/93 $6.00 + 0.00

Numerical study on heat and mass transfer in a liquid-fueled gas turbine combustor

H. K. MA, F. H. LEE and M. W. WANG
Mechanical Engineering Department, National Taiwan University, Taipei, Taiwan, R.O.C.

(*Received* 7 *December* 1992)

Abstract—A two-dimensional spray combustion code is developed for investigating the spray flame in a gas turbine combustor. The modified K–ε model is used to describe the turbulent flow field and the generalized Rosin–Rammler equation is used to evaluate the fuel droplet size distribution in the spray. The effects of the inlet turbulent kinetic energy K_0 and dissipation rate ε_0 on the flow velocity and the length of recirculation zone are studied. Compared with results in the isothermal flow, the recirculation strength will increase, but the length of the recirculation zone will decrease in reacting flow case. Also, the influence of bluff-body size on velocity, temperature, fuel/oxygen concentration, and droplet distribution profiles is studied in detail.

INTRODUCTION

PREVIOUSLY the design of combustors has relied almost exclusively on empirical methods. Increasing the numerical analysis of the fluid flow in the vicinity of the combustors will help further modifications in combustor geometry. Turbulent diffusion flame stabilized by a bluff-body combustor are common in combustion systems. The fuel and air jets are separately admitted into the combustion chambers and the combustion processes are governed by the mixing rate of the two streams. During the mixing process, there is transfer of mass, momentum and energy between the two jets and also between the jets and the ambient air surrounding the bluff-body combustor. There are many ways to make recirculation zones in combustors, to enhance the mixing of fuel and air, which hold the flame without extinguishing it. The simplest way is to change the geometry of the combustors, such as axisymmetric sudden-expansion combustors, or bluff-body type combustors.

Onuma *et al.* [1, 2] found from experiments that the region where droplets exist is limited to a small area around the burner nozzle. And, most of the droplets in the flame do not burn individually, but fuel vapor from the droplets concentrates and burns as a gas diffusion flame. Style and Chigier [3] also found the spray combustion flames and gas diffusion flame are similar in structure. Habib and Whitelaw [4, 5] measured the velocity characteristics and Reynolds-stress tensor of different velocity ratio, with and without swirl. Khalil *et al.* [6, 7], compared different inlet velocity profiles and inlet turbulent kinetic energy K_0 and found that K_0 has a significant effect on velocity distribution. Nikjooy and Mongia [8] compared different profiles of inlet turbulent dissipation rate, and found that it had a strong influence on velocity distribution.

The difference between isothermal and combusting flow characteristics had been investigated by many investigators. Baker *et al.* [9] compared mean velocity and turbulent kinetic energy. Gray *et al.* [10] found that the effects of wall static pressure rise, total pressure decay and velocity decay were reduced by reacting as compared to isothermal flow. Robert and John [11] found the reattachment length was shorter in combusting flow. Bicen and Jones [12] and Heitor and Whitelaw [13] investigate experimentally the recirculation zone in combustion flow which would increase in strength but decrease in width, and the flow was essentially Reynolds number independent for Reynolds number larger than 5×10^4.

The numerical studies of gaseous turbulent diffusion flames mostly used the k–ε turbulence model and one-step chemical reaction, such as Gosman *et al.* [14] who used eddy-break-up combustion model and flux method radiation model. Khalil *et al.* [6, 15] compared the three combustion models and found that two-delta and eddy-break-up models were more accurate. Nikjooy *et al.* [16] used Farve averaged density-weighted method to calculate variable-density flows and low-Reynolds number model to calculate the near-wall region and compared them with experimental data. However, the above numerical studies of turbulent, reactive axisymmetric combustor flows are all with gaseous fuel. The main difficulty of prediction of the characteristics of liquid spray flames is associated with the modeling of the interaction between two phases. Chiu *et al.* [17, 18] developed a group combustion number, Gc, to characterize group combustion occurrences or individual droplet burning. Correa and Sichel [19] developed another parameter to distinguish whether group combustion occurs or not. Whitelaw and Banhawy [20] and Chiu and Zhou [21] considered the droplets as 'sources' of mass, momentum and energy to the gas field. The liquid droplets act as distributed sources of fuel vapor and the influence of the droplets on the gas field were considered through source terms. Whitelaw and Banhawy predicted the flow properties

NOMENCLATURE

a, b, s, t spray parameters
B transfer number
C specific heat at constant volume
C_p specific heat at constant pressure
f_n generalized Rosin–Rammler spray function
f flow flux
G group combustion number
h total enthalpy
h_t thermal enthalpy
J heat equivalence of work
K turbulent kinetic energy
L characteristic length of recirculation
L_h latent heat of vaporization
l turbulence scale
m evaporization rate of spray
N_1 total droplet number density
q heat value of fuel [kcal kmol^{-1}]
R_{se} radius of combustor
r_c droplet radius
S stoichiometric oxygen/fuel ratio, source term
W molecular weight
Y species concentration as mass fraction.

Greek symbols
Γ Γ-function; transport coefficient
ε turbulence dissipation rate
ξ any flow variable
θ droplet void-deducted volume ratio
λ heat conductivity
μ viscosity
ρ density
ϕ mixture fraction
ϕ_r ln $(1+B)$
ψ ratio of droplet turbulent Schmidt number to its gas counterpart.

Subscripts
b boiling point
f fuel
g gas
k kth size group of droplets
l liquid
0 initial or inlet condition
ox oxygen
p product.

of an axisymmetric sudden-expansion combustor with swirl and compared them with experimental data. The results showed that general features of the flowfield were correct except at near-combustor locations and combustion chamber centerline. Chiu and Zhou compared the influence of different inlet conditions such as temperature, pressure and droplet size on combustion efficiency and compared the structure of spray flames associated with group combustion number. The present calculation is mostly based on the governing equations of Chiu and Zhou [21] to predict the characteristics of spray flames in an axisymmetric sudden-expansion combustor.

MATHEMATICAL FORMULATION

A cylindrical spray combustion chamber equipped with a bluff-body combustor was used in this study (cf. Fig. 1). The expansion ratio is defined as R_c/R_3. And, the buff-body ratio is defined as $(R_2-R_1)/R_c$. The normalized conservation equations for the gas phase variables and the droplet number densities are written in the general form as

$$\frac{1}{\bar{r}}\left(\frac{\partial}{\partial\bar{x}}\left(\bar{r}\bar{f}_x\bar{\xi}-\bar{r}\bar{\gamma}\frac{\partial\bar{\xi}}{\partial\bar{x}}\right)+\frac{\partial}{\partial\bar{r}}\left(r\bar{f}_r\bar{\xi}-\bar{r}\bar{\gamma}\frac{\partial\bar{\xi}}{\partial\bar{r}}\right)\right) = S\xi_1+S\xi_2. \quad (1)$$

The normalized concentration equations for the droplet variables and temperature are written as

$$\frac{1}{\bar{r}}\left(\frac{\partial}{\partial\bar{x}}\left(\bar{r}\bar{f}_x\bar{\xi}+\frac{\partial}{\partial\bar{r}}(\bar{r}\bar{f}_r\bar{\xi})\right)-\frac{\bar{\xi}}{\bar{r}}\left(\frac{\partial}{\partial\bar{x}}(r\bar{f}_x)+\frac{\partial}{\partial\bar{r}}(\bar{r}\bar{f}_r)\right)\right)=S\xi_2. \quad (2)$$

$S\xi_1$ and $S\xi_2$ [27] are the innerphase and interphase terms, respectively.

Initial and boundary conditions:

Entrance:

$$\frac{U_g}{U_{go2}}=(1-\bar{r})^{1/7};\quad \bar{V}_g=0$$

$$K_{in}=0.005(U_{go2})^2$$

$$\varepsilon_{in}=C\mu\cdot K^{3/2}/(0.03R_{se}).$$

Exit:

$$\frac{\partial\bar{u}}{\partial\bar{x}}=0;\quad \bar{v}=0;\quad \frac{\partial\bar{\xi}}{\partial\bar{x}}=0$$

where $\bar{\xi}=\bar{k},\bar{\varepsilon},\bar{h},\bar{\phi},\bar{G},\bar{v}_{d.k},\bar{n}_{d.k}$.

Impermeable wall:

$$\left(\frac{\partial\bar{\xi}}{\partial\bar{r}}\right)_\omega=0 \text{ (except } \bar{\xi}=\bar{U}_g)$$

$$(\bar{U}_g)_\omega=(\bar{V}_g)_\omega=0.$$

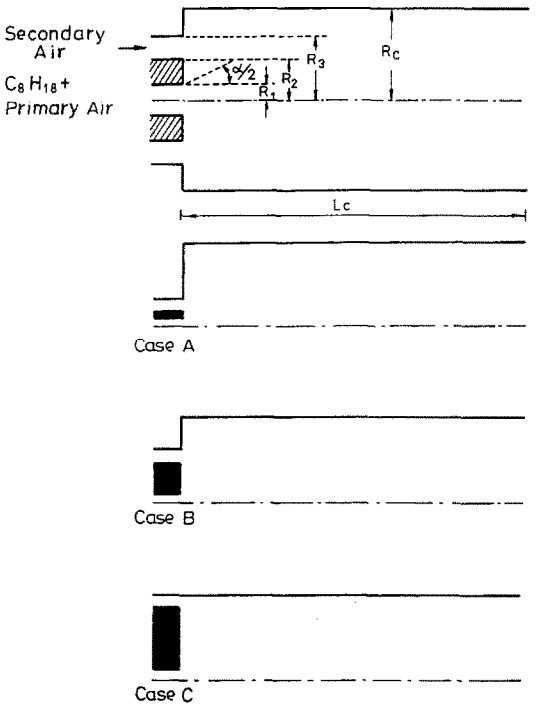

FIG. 1. Schematic of combustor with bluff-body.

Axisymmetric axis:

$$\left(\frac{\partial \bar{\xi}}{\partial \bar{r}}\right)_{\text{axis}} = 0; \quad \bar{V}_g = 0.$$

To render complex phenomena in the spray combustion mathematically manageable, the following assumptions are made in this study:

(1) The spray process is quasi-steady.
(2) There is no nucleation, collision, break-up, coagulation and microexplosion of droplets.
(3) One-step chemical reaction is assumed.
(4) The diffusion coefficients are the same for all species, and the Lewis number is unity.
(5) Droplets are spherically symmetric. There is no internal circulation taking place within droplets. Droplets begin to evaporate only after their temperatures reach the boiling point.
(6) Body and buoyancy forces are neglected.
(7) Radiation heat transfer is not considered.
(8) Ignition does not take place in the liquid phase.

Spray model

The generalized Rosin–Rammler equation is used to evaluate the droplet size distribution in the spray. The droplet number density, N_1, is described by:

$$N_1 = \int_0^\infty f_{n.1}\, \mathrm{d}r_1 \tag{3}$$

where

$$f_{n.1} = \frac{N_1 S}{r_{1m}} \frac{\Gamma[(t+4)/s]^{(t+1)/3}}{\Gamma[(t+1)/s]^{(t+4)/3}} \left(\frac{r_1}{r_{1m}}\right)^t \times \exp\left\{-\left(\frac{r_1}{r_{1m}}\right)^t \left(\frac{\Gamma[(t+4)/s]}{\Gamma[(t+1)/s]}\right)^{s/3}\right\} \tag{4}$$

r_{1m} is the volume mean radius of the droplet.

Parameters s and t are experimentally determined by the numerical solution procedure, and the component droplet number density $N_{1.k}$ is introduced and used instead of $f_{n.1}$ to calculate for the properties of the kth size droplet group in the spray.

$$N_{1.k} = \int_{r_{1.k-1/2}}^{r_{1.k+1/2}} f_{n.1}\, \mathrm{d}r_1.$$

The dimensionless droplet number density of kth group, $\bar{N}_{1.k}$ is defined as

$$\bar{N}_{1.k} = \frac{N_{1.k}}{N_{1.0}} = \frac{\text{droplet number density of } k\text{th group}}{\text{inlet number density (No./cc)}}.$$

Droplet evaporation and combustion model

According to the classical theory, the rate of evaporation of droplet is given by

$$\frac{\mathrm{d}r_1}{\mathrm{d}t} = \frac{-\lambda}{\rho_1 C_p} \frac{N_u \Phi_r}{r_1} \tag{5}$$

where

$$N_u = 1 + 0.276 R_e^{1/2} S_c^{1/3}$$

$$\Phi_r = \ln(1+B)$$

$$B = \frac{1}{L_h}\left(\int_{T_b}^{T_g} C_p\, \mathrm{d}T\right).$$

In this study, liquid droplets are evaporated and do not burn. Ignition and combustion flame occur only in fuel vapor phase.

Turbulent droplet dispersion model

Droplet dispersion represented by the double correlation of the fluctuations of droplet number density and the velocity is presented as follows:

$$\overline{\delta_{n1}\delta V_g} = -\frac{\mu t}{\rho_g \sigma_g} \nabla n_1 \tag{6}$$

$$\overline{\delta_{n1}\delta V_1} = -\frac{\mu t}{\rho_g \sigma_{n1}} \nabla n_1 \tag{7}$$

where $\sigma_{n1} = \sigma_g \psi$, σ_g is Schmidt number of gas.

$$\psi = \sum_{n=0}^{4} a_n (\xi r_1)^n$$

is a part of power series, where

$$\xi = \left(\frac{\rho_1}{\rho_g^{3/4}}\right)^{1/2} \left(\frac{\varepsilon}{k}\right)^{1/2} \tag{8}$$

$a_0 = 1$ and $a_1 \sim a_4$ are decided by experiment.

Modified K–ε model

In the present study, it is assumed that droplets themselves do not produce turbulent kinetic energy; they simply share the energy with the gaseous flow.

In the modified K–ε model, the ε-equation remains invariant though the K-equation has been changed to cover the turbulent kinetic energy of the droplets.

• The turbulence energy K-equation

$$\frac{\partial}{\partial x}\left(\theta\rho_g U_g K-\frac{\theta\mu_{\text{eff}}}{\sigma_K}\frac{\partial k}{\partial x}\right)+\frac{1}{r}\frac{\partial}{\partial r}\left(r\theta\rho_g V_g K-\frac{r\theta\mu_{\text{eff}}}{\sigma_K}\frac{\partial k}{\partial r}\right)=\theta\mu_{\text{eff}}G_k-\theta\rho_g\varepsilon-\int_0^{r}\frac{4}{3}\pi r^3\sigma_{1,k}\left[\frac{\partial}{\partial x}(rf_{n1,k}U_{1,k})+\frac{1}{r}\frac{\partial}{\partial r}(rf_{n1,k}V_{1,k}K_{1,k})\right]\mathrm{d}r_{1,k} \quad (9)$$

where $K_1 \sim K/\psi^2$

$$G_k=\left[2\left(\frac{\partial U_g}{\partial x}\right)^2+2\left(\frac{\partial V_g}{\partial r}\right)^2+2\left(\frac{V_g}{r}\right)^2+\left(\frac{\partial U_g}{\partial x}+\frac{\partial U_g}{\partial r}\right)^2\right]$$

where $\mu_{\text{eff}}=\mu_t+\mu$, μ_t is the turbulent viscosity.

The last term on the right-hand side of equation (9) represents the turbulent kinetic energy of the liquid droplets.

• The multiphase energy dissipation ε-equation

$$\frac{\partial}{\partial x}\left(\theta\rho_g U_{g\varepsilon}-\frac{\theta\mu_{\text{eff}}}{\sigma_\varepsilon}\frac{\partial\varepsilon}{\partial x}\right)+\frac{1}{r}\frac{\partial}{\partial r}\left(r\theta\rho_g V_{g\varepsilon}-r\frac{\theta\mu_{\text{eff}}}{\sigma_\varepsilon}\frac{\partial\varepsilon}{\partial r}\right)=C_1\theta\mu_{\text{eff}}\frac{\varepsilon}{K}\cdot G_k-C_2\theta\rho_g\varepsilon^2/K. \quad (10)$$

The coefficients C_1 and C_2 are constants which are assigned the value $C_1=1.44$ and $C_2=1.92$ [26].

Combustion model

In this model, the mixture consists of the fuel, oxygen and product. And, the chemical reaction rate is so high that the momentary chemical equilibrium is reached everywhere. From the viewpoint of time-averaged concentrations of fuel and oxygen, the reaction rate is finite, due to the turbulent fluctuation of concentration that exists.

(a) Time average mixture fraction concentration

$$\frac{1}{r}\frac{\partial}{\partial r}(r\theta\rho_g V_{g\phi})+\frac{\partial}{\partial x}(\theta\rho_g U_{g\phi})=\frac{1}{r}\frac{\partial}{\partial r}\left(r\theta\frac{\mu_{\text{eff}}}{\sigma_\phi}\frac{\partial\phi}{\partial r}\right)+\frac{\partial}{\partial x}\left(\theta\frac{\mu_{\text{eff}}}{\sigma_\phi}\frac{\partial\phi}{\partial x}\right)+C_\phi\dot{m}_1. \quad (11)$$

(b) The mean square of the mixture fraction concentration

$$\frac{1}{r}\frac{\partial}{\partial r}(r\theta\rho_g V_g G)+\frac{\partial}{\partial x}(\theta\rho_g U_g G)=\frac{1}{r}\frac{\partial}{\partial r}\left(r\theta\frac{\mu_{\text{eff}}}{\sigma_0}\frac{\partial G}{\partial r}\right)+\frac{\partial}{\partial x}\left(\theta\frac{\mu_{\text{eff}}}{\sigma_0}\frac{\partial G}{\partial x}\right)+C_{g1\theta}\frac{\mu_t}{\sigma_0}\left(\frac{\partial\phi}{\partial x}+\frac{1}{r}\frac{\partial\phi}{\partial r}\right)^2-C_{g2\theta}\rho_{g\varepsilon}G/K-\dot{m}_1 G. \quad (12)$$

Equations (11) and (12), treated by Battlement probability density distribution [16] (2 delta pdf function), constituted the core of the turbulent diffusion flame model. The probability density function is assumed. The values of Y_F, Y_{ox}, T and the other thermodynamic properties are calculated from the known ϕ and G.

NUMERICAL METHOD

The generalized forms of elliptic partial differential equations (1) and (2) are discretized into approximate algebraic forms by integrating them over the computational cells within the combustor. A staggered grid system is adopted with all scalar quantities evaluated at the nodal points of the cells and gas velocity components are evaluated at the cell faces [24]. For the calculation of fluxes across the boundary faces special treatment is adopted along the boundaries. Infinitely thin control volumes are introduced to establish conservation of fluxes on the boundaries. The wall functions are used in the near-wall regions in order to bridge these regions where the effects of the molecular viscosity dominate the near-wall.

The SIMPLER procedure [24, 26] is employed to solve for the gas phase flow field. And the power law scheme is used to calculate the combined convection/diffusion fluxes through the interfaces of the control volumes, whereas the upwind scheme is used to calculate the fluxes in the droplet phase, which lacks the diffusion-like terms. With the form of equation (2) in the staggered system, the line-by-line TDMA method is adopted to solve the algebraic equations simultaneously. The solution is augmented by the block correction technique [26], which improves solution convergence. The relaxation factor has been taken at a value below 0.8.

RESULTS AND DISCUSSION

The parametric studies examine the combustion characteristics, spray flame structure, and may establish a guide for the design of spray combustors with higher combustion efficiency. N-Octane (C_8H_{18}), chosen for this study, is a monocomponent fuel. It has a physical–chemical characteristic similar to that of aviation kerosene.

1. *Isothermal flow study*

(a) *The influence of inlet turbulent kinetic energy K_0 and turbulent dissipation rate ε_0.* Turbulent intensities

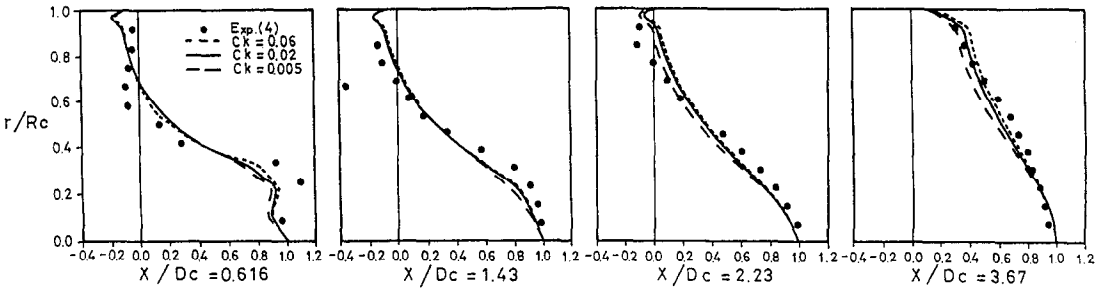

FIG. 2. Influence of inlet turbulent kinetic energy coefficient C_k on mean axial velocity: isothermal flow.

of inlet streams are not always known. In K–ε modified model, the turbulent viscosity μ_t in relationship with K and ε could be represented as $\mu_t = C\mu\rho K^2/\varepsilon$. Thus, the increase of turbulent viscosity μ_t and the decrease of turbulent dissipation rate ε both will increase the effective turbulent viscosity μ_{eff} ($\mu_{\text{eff}} = \mu_t + \mu_l$). In general, the inlet turbulent kinetic energy K_0 could be written as $K_0 = C_k U_0^2$. C_k is the coefficient of inlet turbulent kinetic energy. Figure 2 illustrates the effect of inlet turbulent C_k on the mean axial velocity profiles. The results show that higher C_k value (0.06) will cause an increase of turbulent viscosity and have better agreement with experimental data at $X/D = 3.67$ near-centre region. However, lower C_k value (0.005) will have better agreement near-wall region. Figure 2 also reveals that increasing C_k value will cause a shorter recirculation zone at the corner.

The inlet turbulent dissipation rate ε_0 is calculated from equation $\varepsilon_0 = C\mu K^{3/2}/(LW)$. For smaller characteristic length of recirculation zone (L), the ε_0 will have a larger value and thus decrease the value of turbulent viscosity. The influence of L on centre-line distribution of mean axial velocity will obviously be in the upstream region, especially at $X/D_e = 1.0$. In general, the suitable choice of K_0 and ε_0 are needed due to their effects on the prediction of the isothermal flow velocity and the length of recirculation region.

(b) *The influence of other parameters.* The influence of inlet velocity profile on centre-line distribution of mean axial velocity is not obvious for both uniform and 1/7th law cases [27]. Figure 3 illustrates the influence of expansion ratio, Reynolds number, turbulent kinetic energy coefficient, and mixing length on length of recirculation zone. The length of recirculation zone ($LCRZ$) is proportional to expansion ratio. And, the parameters R_e and L have influence on the $LCRZ$, especially at $R_e < 1.0 \times 10^5$ and $L < 1.0 \times 10^{-2}$. In turbulent region ($R_e > 8.0 \times 10^4$), $LCRZ$ is independent of R_e number.

2. *The comparison of isothermal flow and reacting flow*

The operating conditions, listed in Table 1, are used by comparison with the flow characteristics of isothermal and reacting flow. Both velocity distribution and wall static pressure of isothermal and reacting flow are analyzed as follows:

(a) *Velocity distribution.* The gases in a reacting, recirculating flow mix more slowly than those in an isothermal flow of the same burner configuration and fuel/air ratio. Figure 4 shows that chemical heat addition broadens the mean axial velocity profiles and reduces the axial velocity decay. Figure 5 shows a comparison of the contour plots of axial velocity for reacting and isothermal flow. The reacting flow will have shorter recirculation zone than the isothermal flow. The decay of the length of recirculation zone is due to the thermal expansion downstream and thus increases the strength of the circulation.

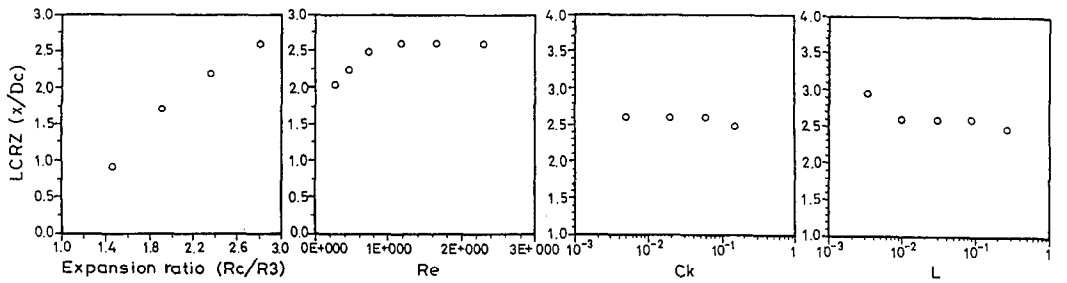

FIG. 3. Influence of expansion ratio, Reynolds number, turbulent kinetic energy coefficient, and mixing length on length of the recirculating zone.

Table 1. Operating conditions

(a) Isothermal flow case

U_{g01} (m s^{-1})	T_{g01} (K)	U_{g02} (m s^{-1})	T_{g02} (K)	p_{g0} (kg cm^{-2})	ρ_{g0} (kg m^{-3})	U_{g0} (kg m^{-1} s^{-1})	Re_1	Re_2
33.04	293	33.04	293	1.001	1.201	1.8×10^{-5}	35 500	50 500

(b) The comparison of isothermal and reacting flow case

Isothermal flow

U_{g01} (m s^{-1})	T_{g01} (K)	U_{g02} (m s^{-1})	T_{g02} (K)	p_{g0} (kg cm^{-2})	ρ_{g0} (kg m^{-3})	U_{g0} (kg m^{-1} s^{-1})	Re_1	Re_2
33.0	600	33.0	700	1.0	0.503	3.3×10^{-5}	10 467	11 536

Reacting flow

Y_{ox01}	Y_{ox02}	U_{do} (m s^{-1})	T_{do} (K)	N_{do} (No. cc^{-1})	r_{dm} 10^{-6} (m)	$(\alpha/2)$
0.0	0.18	25	298	3000	25	20°

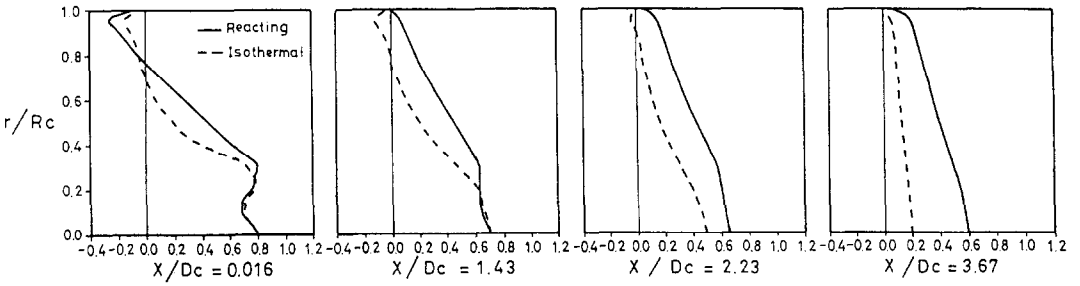

FIG. 4. Radial profiles of axial velocity for reacting and isothermal flow.

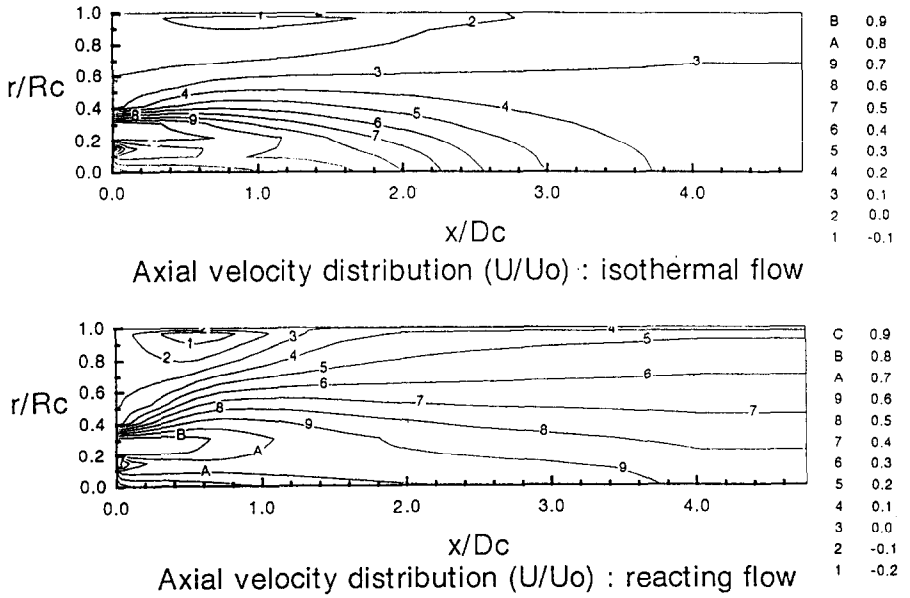

FIG. 5. Contours of axial velocity for reacting and isothermal flow.

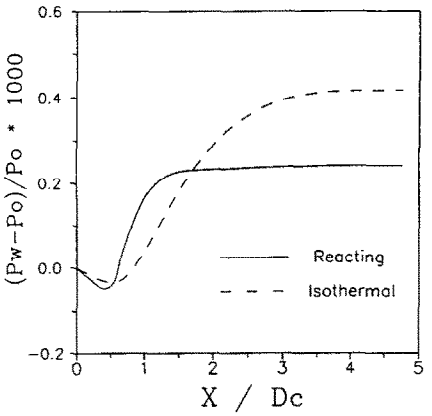

FIG. 6. Axial distribution of wall static pressure.

(b) *Wall static pressure.* The axial distribution of wall static pressures is shown in Fig. 6. The pressure indicates that the one significant effect which the chemical heat release has on the recirculating flowfield is to raise the rate of wall static pressure for $1.5 > X/D > 0.5$; for X/D greater than 1.5, the pressure decay is slowed down by the chemical heat addition. The effect of the chemical reaction is to reduce the rate of momentum transport between the two coaxial streams. This phenomenon agrees with the test results of Gary *et al.* [10].

Table 2. Parametric studies

Case	R_1	R_2	R_3	R_c	R_c/R_3	$(R_2-R_1)/R_c$
A	0.805	1.08	2.225	6.25	2.81	0.044
B	0.805	2.88	4.025	6.25	1.55	0.332
C	0.805	5.105	6.25	6.25	1.0	0.688
D	0.805	1.88	3.025	6.25	2.07	0.288
E	0.805	3.88	5.025	6.25	1.24	0.492

3. *Parametric studies in reacting flow*

Five cases, listed in Table 2, are studied. But, three cases (*A*, *B*, *C*) are shown in Fig. 1 and compared with results.

(a) *The length of recirculation zone.* In Fig. 7, recirculation zones are formed at the corner and behind the bluff-body. Case *C* is a limiting case without corner recirculation. Figure 8 shows the effect of expansion ratio and bluff-body size ratio on the length of recirculation zone at the corner or behind the bluff-body for both isothermal and reacting flow cases. The result

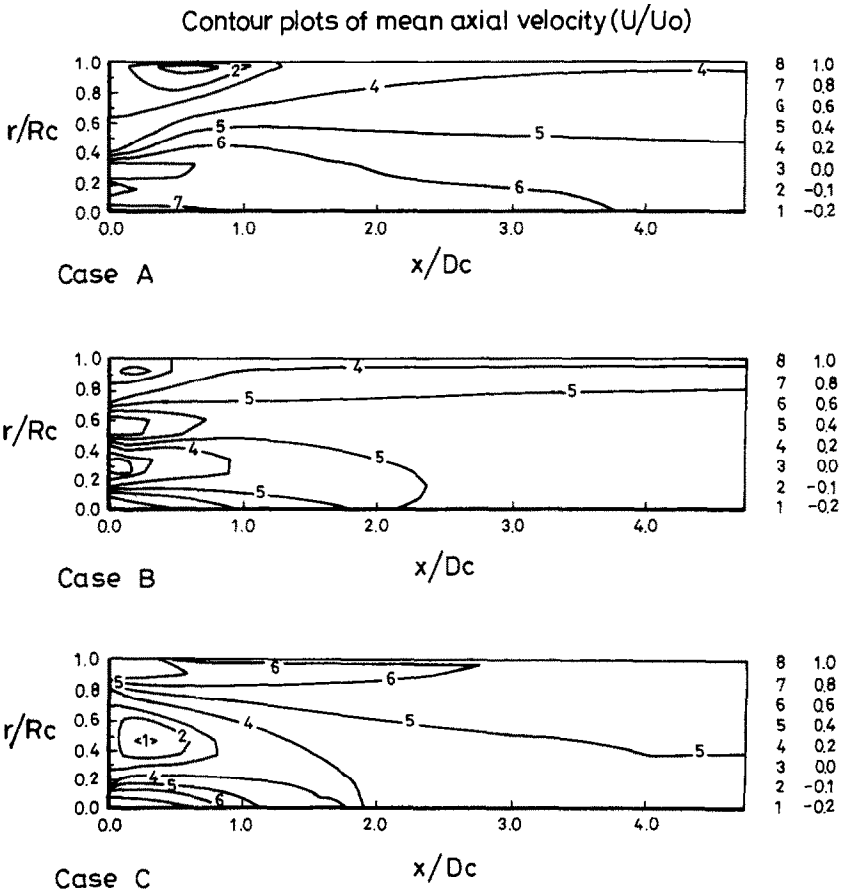

FIG. 7. Contours of axial velocity for three different cases.

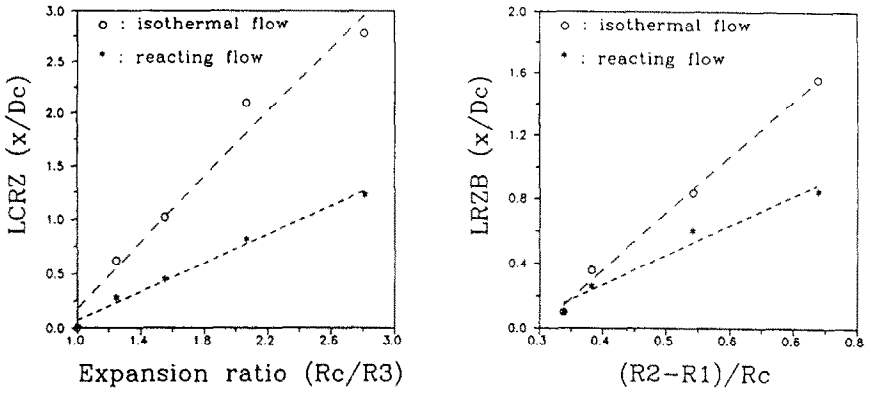

FIG. 8. The length of recirculation zone vs expansion ratio and bluff-body size ratio.

shows the length of recirculation zone at the corner is proportional to the expansion ratio (R_c/R_3). Similarly, the length of the recirculation zone behind the bluff-body is also in proportion to bluff-body ratio $(R_2-R_1)/R_c$. The results reveal that the reacting flow will have a shorter recirculation zone than the isothermal flow. The decay of the length of the recirculation zone is due to thermal expansion downstream and thus increases the strength of the circulation. For the length of recirculation zone at the corner, the slope ratio of reacting flow/isothermal flow is 0.43. And, for the length of recirculation zone behind the bluff-body, the slope ratio of reacting flow/isothermal flow is 0.48.

(b) *Expansion ratio*, R_c/R_3. Increasing expansion ratio will enlarge the upstream recirculation zone around the corner (cf. Fig. 7) and decrease the accumulation of droplets at the downstream wall (cf. Fig. 9). The accumulation of droplets at wall ($r/R_c = 1.0$) is caused by stick-evaporation model, which was used in this study. In Fig. 9, the group size numbers $K = 1, 2, 3, 4$ are represented as 11.0, 18.0, 25.0 and 33.0 μm, respectively, when the initial mean

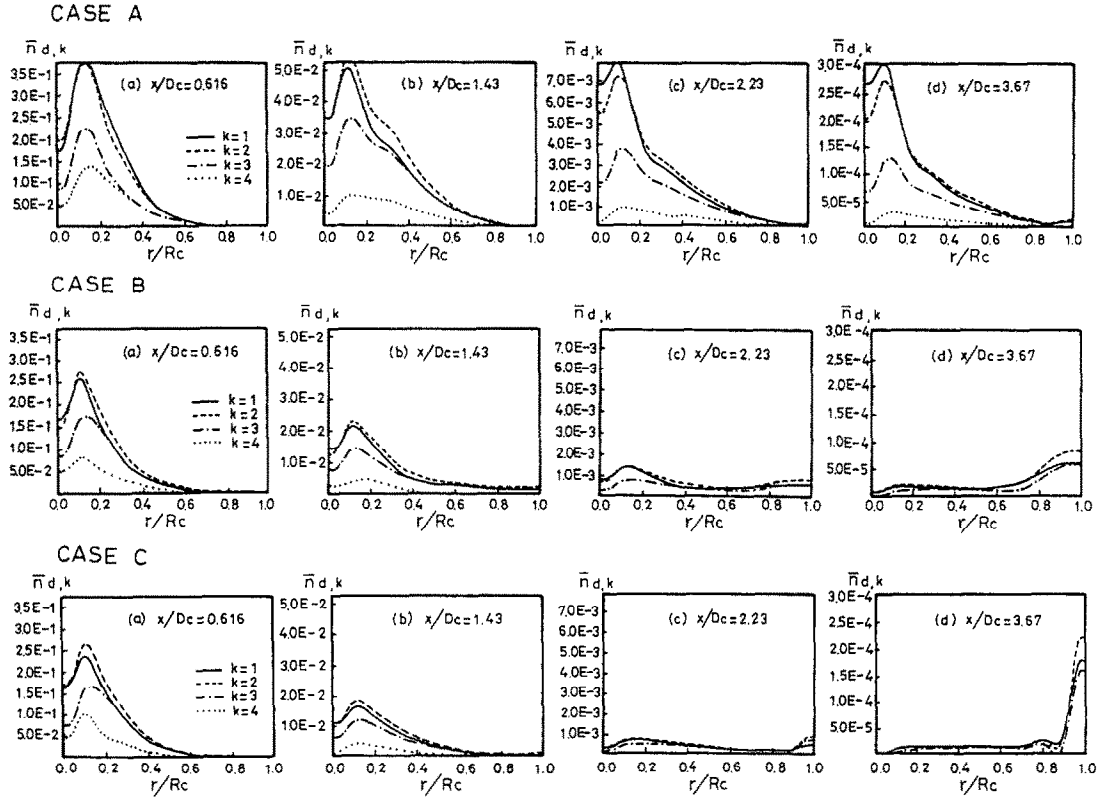

FIG. 9. Distribution of droplet number density at $x/D_c = 0.616$, 1.430, 2.230 and 3.670.

diameter is equal to 50 μm. In the spray combustion process, a large droplet will evaporate and burn, and thus decrease in the x-direction. However, larger expansion ratio will induce more pressure drop due to larger aerodynamic expansion loss.

(c) *Bluff-body ratio* $(R_2-R_1)/R_c$. When a bluff-body is placed in the flow of a combustible mixture, a recirculating vortex occurred in the wake of the bluff-body (cf. Fig. 7). If the combusting flow surrounds the recirculation zone, high temperature combusting products will penetrate into the vortex and be carried upstream where they may mix with fresh combustible mixture (cf. Fig. 10). Since the rate of the transfer and mass between the wake and the flow past the wake is high enough to make chemical reaction take place earlier, the evaporation rate of droplet increases and stabilizes the flame. This will be attributed to the higher recirculation flow and increases the exchange of heat and mass transfer between the recirculation zone and the outside surrounding flow, as evidenced by the higher burning rate.

(d) *Temperature profiles*. The group envelope flame structure is characterized by concentration profiles of fuel vapor and oxidizer; both approach to zero near the flame zone. In cases A, the droplets of liquid fuel are sprayed out more. The fuel vapor concentrations exist at the downstream and near-wall region (cf. Fig. 11). And, most of the oxygen concentrations are spray near injector and recirculation zone at the corner. Therefore, the flame zone spray out started from $X/D_c = 1.2$ (cf. Fig. 12). In addition, low vapor concentration is found at the corner recirculation zone. It may account for the non-existing flame at corner zone. Case C is a limiting case with a larger bluff-body (without corner recirculation). A circulating vortex occurred in the wake of the bluff-body. Higher temperature combusting products will penetrate into the vortex and be carried upstream where they may mix with fresh oxidizer. Thus, chemical reactions take place earlier and the flame zone locates near centreline area (cf. Fig. 12). It accounts for ensuring flame stabilization.

CONCLUSIONS

A computer code is developed for predictions of the flow and spray combustion characteristics of a bluff-body combustor. The study on geometrical con-

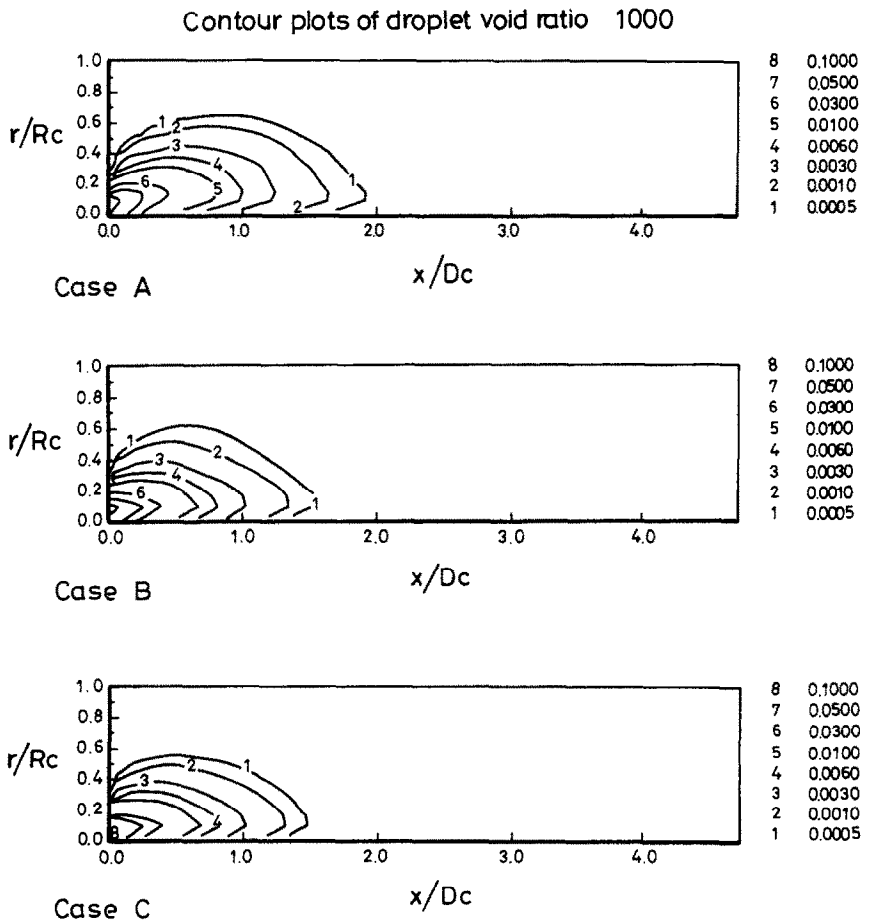

FIG. 10. Contours of droplet void ratio.

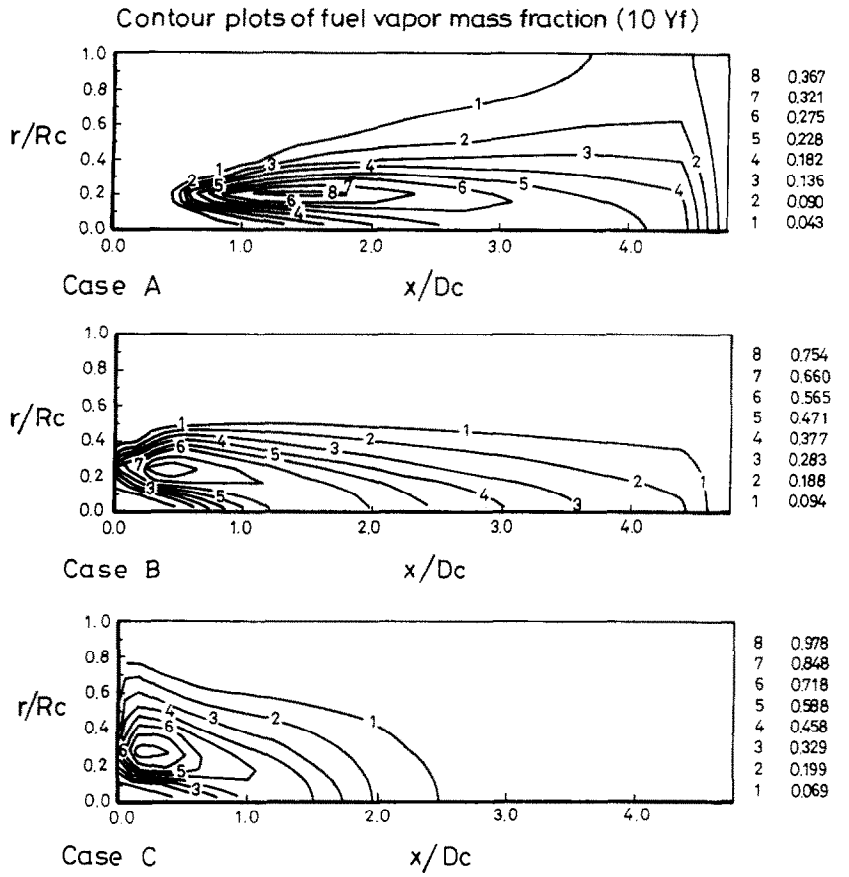

FIG. 11. Contours of fuel vapor concentration (Y_f).

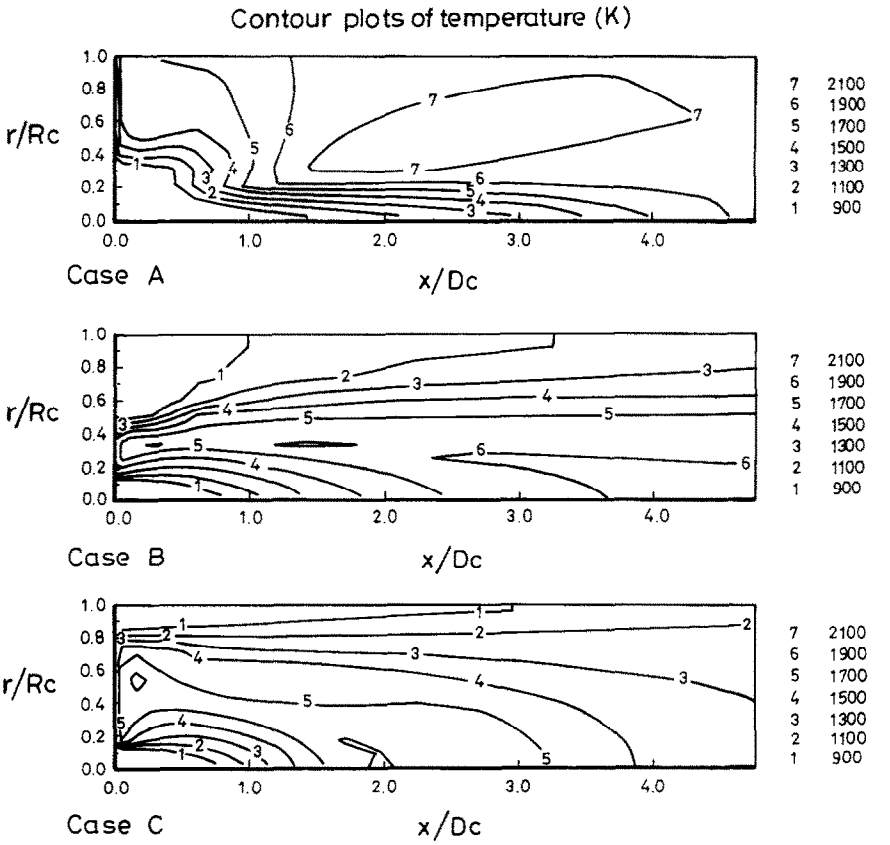

FIG. 12. Contours of temperature (K).

figuration of burners may aid the design and improve the mixing efficiency. The following is a summary of the findings and conclusions.

(1) Inlet turbulent kinetic energy K_0 and dissipation rate ε_0 will affect the effective viscosity coefficient μ_{eff} and thus change the diffusivity value. Increasing inlet K_0 or decreasing inlet ε_0 will cause the shorter recirculation zone at the corner.

(2) The reacting flow will have a shorter recirculation zone than the isothermal flow. The length of recirculation zone at the corner (or behind the bluff-body) is linearly proportional to the expansion ratio or (bluff-body ratio). In comparison of the slope ratio of reacting flow and isothermal flow, the slope ratio is 0.43 for recirculation zone at the corner and 0.48 for recirculation zone after the bluff-body.

(3) In turbulent region ($R_e > 8.0 \times 10^4$), the length of recirculation zone is independent of R_e number. In laminar or transition region ($R_e < 8.0 \times 10^4$), the length of recirculation zone is in proportion to R_e number.

(4) More fuel droplets and vapors exist near the burner when the bluff-body area ratio increases. It accounts for ensuring flame stabilization.

(5) Little fuel vapor is found at the corner recirculation zone. It may account for the non-existing flame at the corner zone.

REFERENCES

1. Y. Onuma and M. Ogasawara, Studies on the structure of a spray combustion flame, *15th Symposium on Combustion*, pp. 453–464 (1975).
2. Y. Onuma, M. Ogasawara and T. Inoue, Further experiments on the structure of a spray combustion flame, *16th Symposium on Combustion*, pp. 561–567 (1977).
3. A. C. Style and N. A. Chigier, Combustion of air blast atomized spray flames, *16th Symposium on Combustion*, pp. 619–630 (1977).
4. M. A. Habib and J. H. Whitelaw, Velocity characteristics of confined coaxial jets with and without swirl, *J. Fluid Engng* **102,** 47–53 (1980).
5. M. A. Habib and J. H. Whitelaw, Velocity characteristics of confined coaxial jets, *J. Fluid Engng* **101,** 521–529 (1979).
6. E. E. Khalil, D. B. Spalding and J. H. Whitelaw, The calculation of local flow properties in two-dimensional furnace, *Int. J. Heat Mass Transfer* **18,** 775–791 (1975).
7. J. S. Philip and L. D. Smoot, Turbulent gaseous combustion. Part 2: theory and evaluation for local properties, *Combust. Flame* **42,** 277–285 (1981).
8. M. Nikjooy and H. C. Mongia, A second-order modeling of confined swirling flow, *Int. J. Heat Fluid Flow* **12**(1), 12–19 (1991).
9. R. J. Baker, P. Hutchinson, E. E. Khalil and J. H. Whitelaw, Measurements of three velocity components in a model furnace with and without combustion, *15th Symposium on Combustion*, pp. 553–559 (1975).
10. D. S. Gray, V. G. Thomas and G. C. Carl, Measurements of reactive recirculating jet mixing in a combustor, *AIAA J.* **21**(2), 270–276 (1983).
11. W. P. Robert and W. D. John, Combustion in a turbulent mixing layer formed at a rearward-facing step, *AIAA J.* **21**(11), 1565–1570 (1983).
12. A. F. Bicen and W. P. Jones, Velocity characteristics of isothermal and combustion flows in a model combustor, *Combust. Sci. Tech.* **49,** 1–15 (1986).
13. M. V. Heitor and J. H. Whitelaw, Velocity, temperature, and species characteristics of the flow in a gas-turbine combustor, *Combust. Flame* **64,** 1–32 (1986).
14. A. D. Gosman, F. C. Lockwood and A. P. Salooja, The prediction of cylindrical furnace gaseous fueled with premixed and diffusion burners, *17th Symposium on Combustion*, pp. 747–759 (1978).
15. E. E. Khalil, P. Hutchinson and J. H. Whitelaw, The calculation of the flow and heat-transfer characteristics of gas-fired furnaces, *18th Symposium on Combustion*, pp. 1927–1939 (1981).
16. M. Nikjooy, R. M. C. So and R. E. Pack, Modelling of jet and swirl stabilized reacting flows in axisymmetric combustors, *Combust. Sci. Tech.* **458,** 135–153 (1988).
17. H. H. Chiu and T. M. Liu, Group combustion liquid droplets, *Combust. Sci. Tech.* **17,** 127–142 (1977).
18. H. H. Chiu, H. Y. Kim and E. J. Croke, Internal group combustion of liquid droplets, *19th Symposium on Combustion*, pp. 971–980 (1982).
19. S. M. Correa and M. Sichel, The group combustion of a spherical cloud of monodisperse fuel droplets, *19th Symposium on Combustion*, pp. 981–991 (1982).
20. Y. E. Banhawy and J. H. Whitelaw, Calculation of the flow properties of a confined kerosene-spray flame, *AIAA J.* **18**(12), 1503–1510 (1980).
21. H. H. Chiu and X. Q. Zhou, Spray group combustion process in air breathing propulsion combustors, *AIAA J.* 83–1323 (1983).
22. D. B. Spalding, Mathematical models of turbulent flames; a review, *Combust. Sci. Tech.* **13,** 3–25 (1975).
23. B. E. Launder and W. P. Jones, The prediction of laminaration with a two-equation turbulence model, *Int. J. Heat Mass Transfer* **15,** 301–314 (1972).
24. S. V. Patankar, *Numerical Heat Transfer and Fluid Flow*. Hemisphere, Washington, D.C. (1980).
25. J. K. Eaton and J. P. Johnson, A review of research on subsonic turbulent flow reattachment, *AIAA J.* **19**(2), 1093–1100 (1981).
26. S. V. Patanker, A calculation procedure for two-dimensional elliptic situations, *Numerical Heat Transfer* **4,** 409–425 (1981).
27. H. K. Ma and M. Y. Wang, A turbulent group spray combustion model of a bluff-body combustor, *The Proceedings of 2nd National Conference on Combustion Science and Technology*, Taiwan (1992).